Published in Catena 59 : 1-17, 2005,
which should be used for any reference to this work

Biologically induced accumulations of $CaCO_3$ in orthox soils of Biga, Ivory Coast

Guillaume Cailleau[a], Olivier Braissant[a], Christophe Dupraz[a], Michel Aragno[b], Eric P. Verrecchia[a,*]

[a] *Institut de Géologie, Université de Neuchâtel, Rue Emile Argand 11, CH-2007, Neuchâtel, Switzerland*
[b] *Laboratoire de Microbiologie, Institut de Botanique, Université de Neuchâtel, Rue Emile Argand 9, C.P. 2, CH-2007 Neuchâtel, Switzerland*

Abstract

Biologically induced accumulations of calcium carbonate have been found inside orthox soils, under and around the native iroko tree *Milicia excelsa* (Moraceae) in Biga (Ivory Coast). The nature of these accumulations and their origin were studied in two soil profiles, directly under the tree and at a distance of 30 cm from the trunk. Microscale forms of $CaCO_3$ include: (1) wood pseudomorphic structures such as parenchyma cells, cellulose fibers, and calcitic vessel infillings; (2) three types of rhombohedra; and (3) needle fiber calcite (NFC). In addition, large scale blocks exhibit three types of textures: (1) micritic calcite, which seems to be the original material; (2) light-colored sparite in moldic voids; and (3) asymmetrical radiaxial laminated fibrous cement. Some micritic aggregates and hemi-spherulites (vaterite) were found in the sap on the trunk as well as in soils on silica grains and the wood itself. The mineralogy of all these carbonate forms is mainly a stoichiometric calcite or a moderately enriched Mg calcite. However, some samples contain monohydrocalcite, as well as two polymorphs of calcium oxalate (weddellite and whewellite). Calcite precipitation is facilitated by the oxidation of oxalate by soil bacteria that contributes to the increase in pH in Biga soils. This is in contrast to conventional orthox soils. Therefore, three conditions are necessary for biologically induced precipitation of calcium carbonate in orthox soils associated with iroko trees: the presence of a large amount of oxalate (originating from the tree and fungi), the existence of an oxalotrophic flora for oxalate oxidation into carbonate, and a dry season.

Keywords: Carbonate accumulations; Iroko tree; Orthox soils; Oxalate; Biomineral

* Corresponding author. Tel.: +41-32-7182600; fax: +41-32-7182601.
E-mail address: eric.verrecchia@unine.ch (E.P. Verrecchia).

1. Introduction

In Ivory Coast, the exotic iroko tree *Milicia excelsa* (Moraceae) grows on orthox soils, which normally have a pH between 4.3 and 6.0 (Leneuf, 1959). Unexpected accumulations of calcium carbonate have been found in, under, and around the trees even though the stable pH for calcite is ≈ 8.4 in these environmental conditions of pressure and temperature. Irokos observed in the study area (northern Ivory Coast, Daloa County) are the remains of a primary rainforest. Today, savanna dominates the region, where most of the observations have been conducted. The iroko trees observed are at least 100 years old and have trunk diameters measuring 2 m on average at 1 m from the ground. These trees are still alive or have been cut by lumberjacks at least at 1 m from the ground because they are extremely mineralized near the ground surface (Braissant et al., 2004). It is not uncommon for chainsaws to be broken during logging operations by "stones" present in the wood. This mineralization was described by Campbell and Fisher (1932), Harris (1933), and Carozzi (1967) who mentioned the presence of calcareous sap, which contributed to form calcite-cemented sandstone around *M. excelsa*. These sandstones are principally located near damaged roots where bicarbonate-bearing sap bleeding occurs. The purpose of this paper is to study: (1) the morphologies of the various calcium carbonate accumulations in the soil, (2) their associated crystallinity and mineralogy, and finally, (3) the relationships between the various types of $CaCO_3$, the iroko, and their distribution under the tree.

2. Geological setting

Orthox soils in Biga (Ivory Coast) have developed on Precambrian calco-alkaline granite and heterogenous granitoide with biotite as parent rocks (Carozzi, 1967; Teeuw, 2002). The Quaternary erosion of the Tertiary peneplanation led to an uneven landscape with a mean elevation between 200 and 300 m asl. The average rainfall is 1500 mm/year and the dry season lasts from December to January. The mean annual temperature is 24.5 °C (FAO, 2001). Field investigations were carried out on two profiles located near the village of Biga (Fig. 1; perimeter 4360 of the "Compagnie Ivoirienne de Bois"). Profile A is located at 30 cm from a hollow iroko trunk of about 2.5 m in diameter, which has been recently cut down (Fig. 2). The profile is 100 cm deep, and has been sampled every 5 cm. Profile B is located below the hollow trunk, and is 100 cm deep. The first 20 cm have not been sampled because they are partially of anthropogenic origin. This profile has been sampled every 10 cm.

3. Materials and methods

Three types of samples have been taken: biomineralized wood on the rootstock, carbonate-rich sap on the trunk, and bulk soil samples from two profiles. In both profiles, two types of carbonate features have been studied: (i) disseminated calcium carbonate features found inside the soft soil, and (ii) mineralized wood fragments and large scale

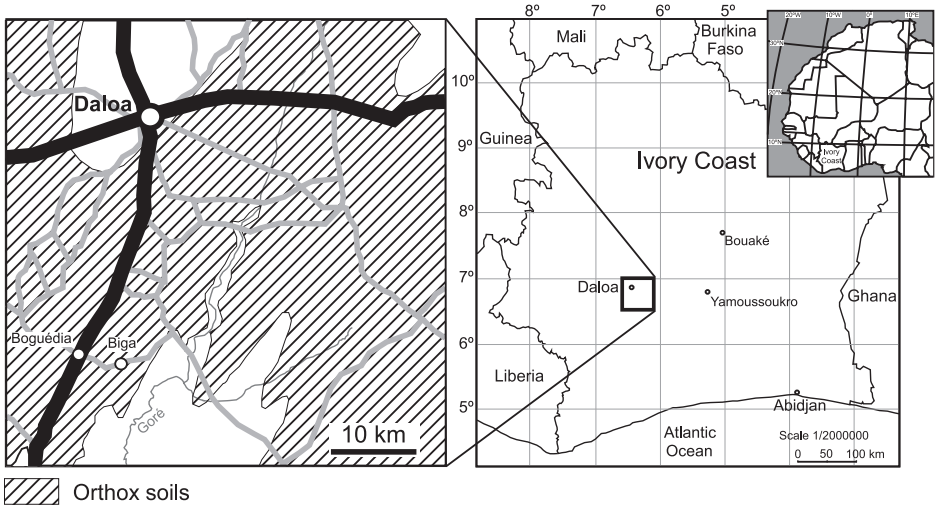

Fig. 1. Maps of the study area showing the extent of orthox soils in which calcium carbonate accumulations have been found.

blocks. Disseminated carbonates were titrated using sulfuric acid (0.5 N) and sodium hydroxide (0.5 N): 1 g of bulk sample has been used if it contained < 50% carbonate by weight. Only 0.5 g has been dissolved if the first titration indicated >50% carbonate by weight. The carbonate content of the second type of feature has been measured by the

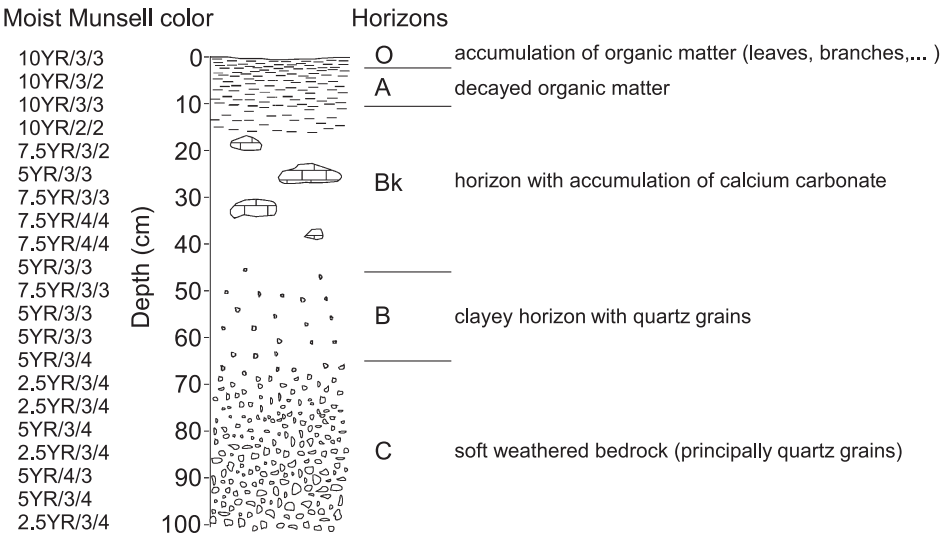

Fig. 2. Reference "pseudo-calciorthid" soil (Profile A at Biga site).

difference between 1 g of original material and the weight of the same material after dissolution in 10% hot hydrochloric acid during 1 h.

In addition, each sample was observed under a binocular microscope. Thin sections have been made of blocks and soft soil samples after resin induration. Observations on some particular features have been made using a Phillips XL30 scanning electron microscope (SEM) including the cryo-scan mode. Systematic X-ray diffraction analysis of carbonates from Profile A has been performed using a Scintag diffractometer. Soil pH_{H_2O} data have been obtained from a solution of 10 g of bulk soil dispersed in 25 ml of deionized water for 16 h. The pH of the resulting solution was measured using a Metrohm Titroprocessor. In order to explain some rhombohedral textures, iroko bark fragments have been burned at 500 °C during 1 h, removed from the oven and left at ambiant air temperature for 2 days.

Two rainfalls have been sampled at the beginning of the wet season. Two soil extracts have been performed (1 kg soil/1 l water) to quantify the labile calcium ion content. Calcium content has been analyzed by liquid chromatography using a Dionex chromatograph with a conductivity detector.

4. Results

Various carbonate features have been found in the soil associated with the iroko tree. They include calcified wood microstructures such as parenchyma cells and cellulose fibers, different types of rhombohedra, needle fiber calcite, large blocks, micritic aggregates, and hemi-spherulites. These features are classified according to their nature and the environment in which they are found. Their mineralogy is discussed when it has been possible to sample them individually. In addition, their distribution along Profile A is presented.

4.1. Mineralized wood tissues

All the fine features have been preserved in the calcified wood pseudomorphic tissues in both profiles. These include mineralized parenchyma cells (Fig. 3A), cellulose fibers (Fig. 3B), and calcitic vessel infillings, (Fig. 3C,D). They are found either individually, dispersed in the soil, or in extremely well-preserved wood tissues (Fig. 3A). Some root samples (up to 1050 g) have a $CaCO_3$ content between 97% and 99%. In Profile A, there are less well-preserved $CaCO_3$ wood pseudomorphic tissues than in Profile B, in which the soil carbonate content can reach up to 63%.

4.2. Rhombohedra

Three types of rhombohedra are distinguished based on their texture. The first type of rhombohedron (Type I) is characterized by smooth crystal faces and has a size $\approx 100-120\,\mu m$ (Fig. 4A). These rhombohedra are found in a polysaccharide-rich medium interpreted as sap by Carozzi (1967). Sampled on the trunk itself, they can also be found in the upper 50 cm of the profile near the trunk or the tree roots, when wounds to the tree caused by wild animals release sap to the surroundings.

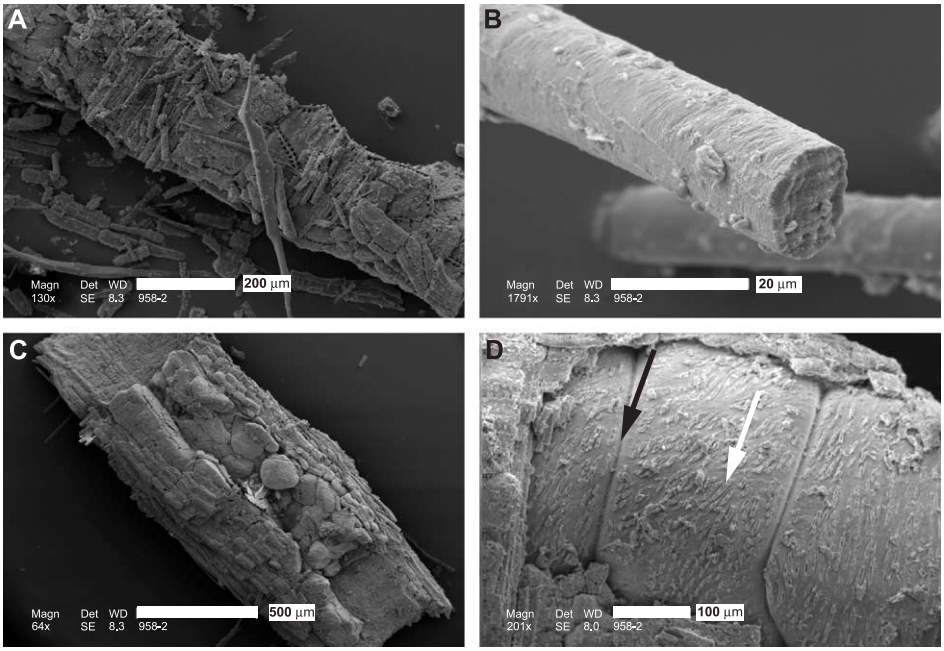

Fig. 3. Scanning electron microscope (SEM) micrographs of mineralized wood structures principally found in Profile B. The mineralized wood has a stoichiometric calcite mineralogic signature. (A) Calcified wood with well preserved cell walls. (B) Wood tissues can be found as large pieces, as well as isolated cellulose fibers. Note the extremely fine preservation of the wood structure during calcite mineralization. (C) Partial conductive vessel infillings showing various crystal morphologies. These vessel infillings can also be found dispersed in the soil. (D) Detail of a conductive vessel infillings. The parietal imprint (white arrow) as well as tyloses (black arrow) are clearly visible.

The second type of rhombohedron (Type II) has been found along Profile A, from the surface to a depth of 70 cm. The size of these rhombohedra ranges from 5 to 70 µm with a mean size of 15 µm (Fig. 4B). These rhombohedra are atypical compared to the more common texture of the Type I rhombohedron. SEM observations show stacking of nanospheres about 200 nm in diameter (Fig. 4C,D) with various stages of coalescence. This specific arrangement induces a significant nanoporosity. The distribution of these nanospheres follows oriented crystallographic planes, typical of the rhombohedral system. Under plane polarized light (PPL), these rhombohedra seem to be composed of micritic grains without showing full extinction under crossed polarized light (XPL).

The third type of rhombohedron (Type III) observed in Profile A occurs below 20-cm depth. The size of these rhombohedra ranges from 30 to 125 µm. SEM observations show crystals with smooth faces (Fig. 4E). Nevertheless, two structures appear under XPL (Fig. 4F): a micritic core, surrounded by a more lighter layer, composed of subhedral crystals ranging from 2.5 to 5 µm in size. SEM observations of a partially broken rhombohedron confirm that the micritic internal structure is composed of the same nanospheres (200 nm in diameter) as Type II crystals. Types II and III rhombohedra

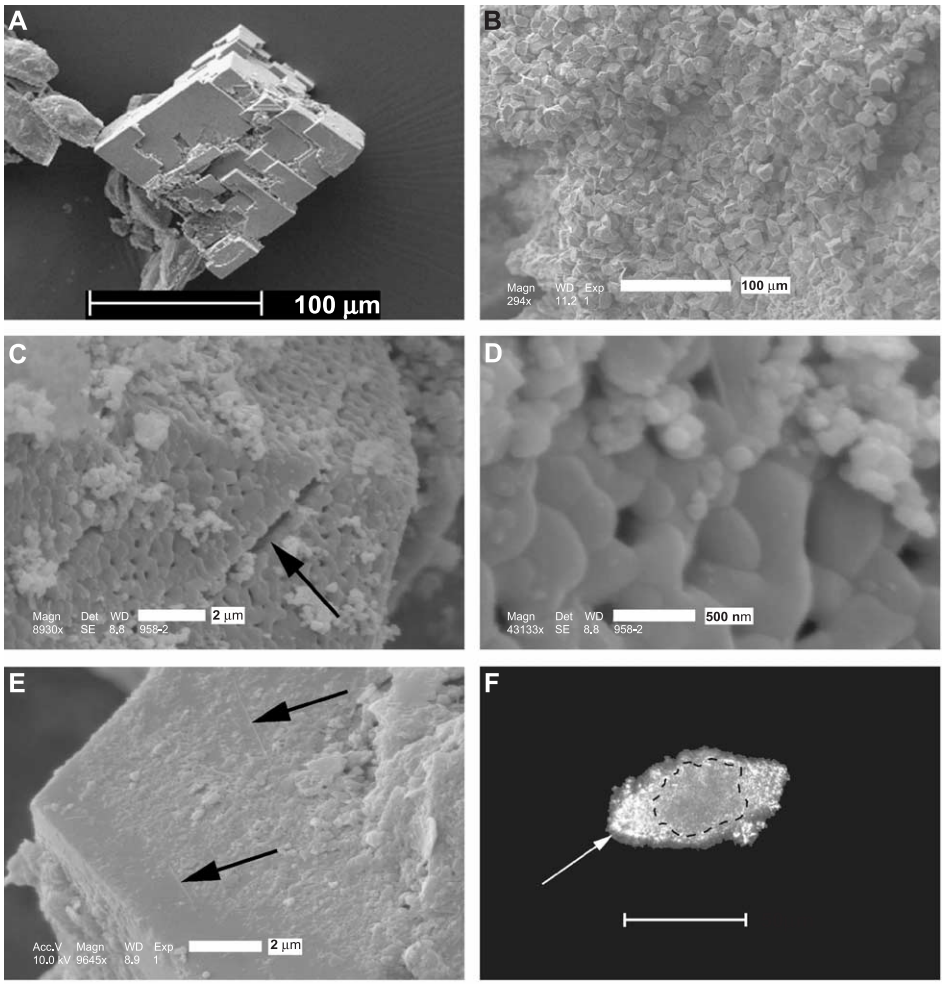

Fig. 4. SEM micrographs of rhombohedral crystal patterns. (A) Type I rhombohedron characterized by smooth faces, found in the sap sampled on the trunk. (B–F) Type II rhombohedra found in the upper part of Profile A. (B) Rhombohedra accumulation in the form of grain coatings in soil vughs. These rhombohedra have various habits. (C) Detail of a rhombohedron surface: faces and edges are well developed despite its atypical texture. Frequently, crystals are fractured (black arrow). (D) Detail of a crystal face composed of coalescent nanospheres ($\approx$ 200 nm in diameter). Note the nanopores between some coalescent nanospheres. (E) Type III rhombohedron with smooth crystal faces, which coexist with Type II rhombohedra. Black arrows show fine long rods, systematically associated with these rhombohedra inside the soil. (F) Cross polarized light (XPL) micrograph: a micritic core (in the area inside the dashed line) composed of nanospheres is surrounded by a lighter layer, corresponding to the smooth and well crystallized faces (white arrow). Bar = 50 micrometers.

coexist at the same depth in the soil. The difference in shape between these three types of rhombohedron is illustrated in Fig. 5 and Table 1, which summarizes their size, structure, porosity, and location.

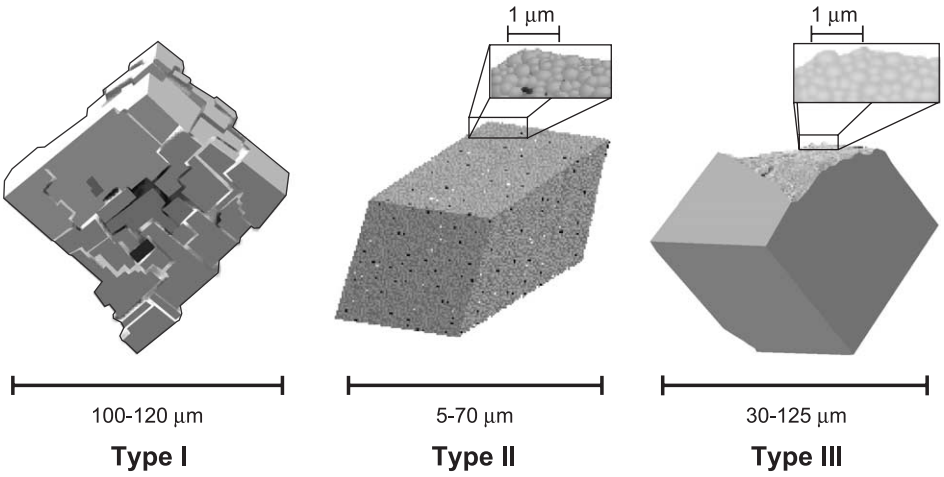

Fig. 5. Three different types of rhombohedra observed at the Biga site.

4.3. Needle fiber calcite

Needle fiber calcite (NFC) is only present in Profile A. NFC can be found in the soil from 30 to 80 cm in depth but is not the most important carbonate feature along the profile in terms of mass. It appears as a coating on quartz and iron oxide grains, sometimes associated to a soil-feeder termitary. At a depth of 80 cm, it is the only calcitic feature observed and consequently chemically titrated. According to the classification of Verrecchia and Verrecchia (1994), the needles (Fig. 6) are identified as: (i) the single M type, described as monocrystalline micro-rods (Fig. 6A, black arrow), is smooth to slightly irregular, with a length of 2–3 μm and a diameter of 100 nm; (ii) the MA type is composed of monocrystalline rods (Fig. 6A, white arrow). These needles are smooth, paired (MA3 and MA4 subtypes), 150–200 μm long and with an average width of 0.4 μm; and (iii) the MAB type (Fig. 6B), which is an evolution of the MA type showing epitactic growth of $CaCO_3$. The latter type starts to form the serrated edge, the structure typical of the MB

Table 1
Differences between the three types of rhombohedra

Rhombohedron type	Type I	Type II	Type II
Size	100–120 μm	5–70 μm	30–125 μm
Shape	Euhedral	Euhedral to subhedral	Euhedral
Structure	Monocrystalline	Stacked nanospheres	Stacked nanospheres with epitactic calcium carbonate infilling nanoporosity
Porosity	No porosity observed	Nanoporosity	No porosity observed
Location	In sap and in the upper 50 cm of soil	In the upper 70 cm of soil	Below 20 cm of soil

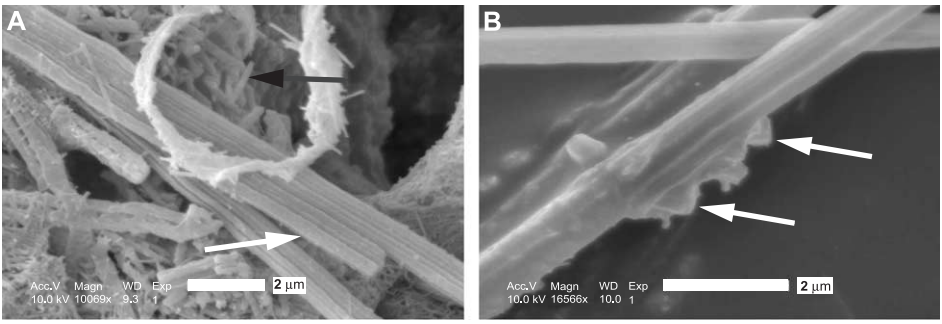

Fig. 6. SEM micrographs of needle fiber calcite at 35-cm depth in Profile A. (A) Cluster of needle fiber calcite in a soft sample. Black arrow: M type microrod; white arrow: paired needle fiber calcite of MA type. The white ring is an organic filament covered with crystals. (B) Needle fiber calcite of MAB type. White arrows: epitactic calcite crystals forming the serrated-edged structure.

type. No MB type has been found in this profile. The least abundant type found in the profile is the MAB type, the two other types (M, MA) constitute most of the NFC found at the Biga site.

4.4. Large blocks of calcium carbonate

Some large scale irregularly shaped blocks of carbonate have been found around the trees. At first, they appear similar to those already observed by Carozzi (1967). The blocks found in this study are maximum 30 cm long and weigh up to 2.3 kg (Fig. 7A). However, Carozzi found hardened blocks " 1–1.5 m in size" (Carozzi, 1967, p. 598).

Thin section observations allow three types of calcite textures to be distinguished: (i) a micritic calcite, which seems to be the original material compared to (ii) a light sparitic calcite. This latter phase is the only feature present in moldic voids (dissolved Gastropods shells) that are not systematically infilled. Nevertheless, both textures coexist irregularly in the matrix of the bulk samples. Except for the moldic voids, the coarse crystals (15–20 to 70 μm) are rich in inclusions, indicating replacement or growth in a pre-existing micrite; (iii) in addition, asymmetrical radiaxial laminated fibrous cement (which is inclusion-free) has also been observed on a matrix (Fig. 7B). An additional texture already described in this paper is the presence of rhombohedra, 80–100 μm in size (Fig. 7C) in some voids. The size, as well as the monocrystalline structure sometimes enriched in inclusions, seems to indicate a Type I rhombohedron.

The observed blocks are not similar to those described by Carozzi (1967), as no quartz grains have been observed in them and calcite is the essential component. In close vicinity to the carbonate blocks, typical orthox material includes some carbonate grains and clusters. This material has only been observed at the external surface and in the outer few first centimeters of the block. Locally, some fans of radiaxial fibrous cement grow from a straight micritic and/or organic line on which other inverted fans grow in the opposite direction. Several of these layers can be observed, always associated with wood features, which are found on the periphery of the sample. These

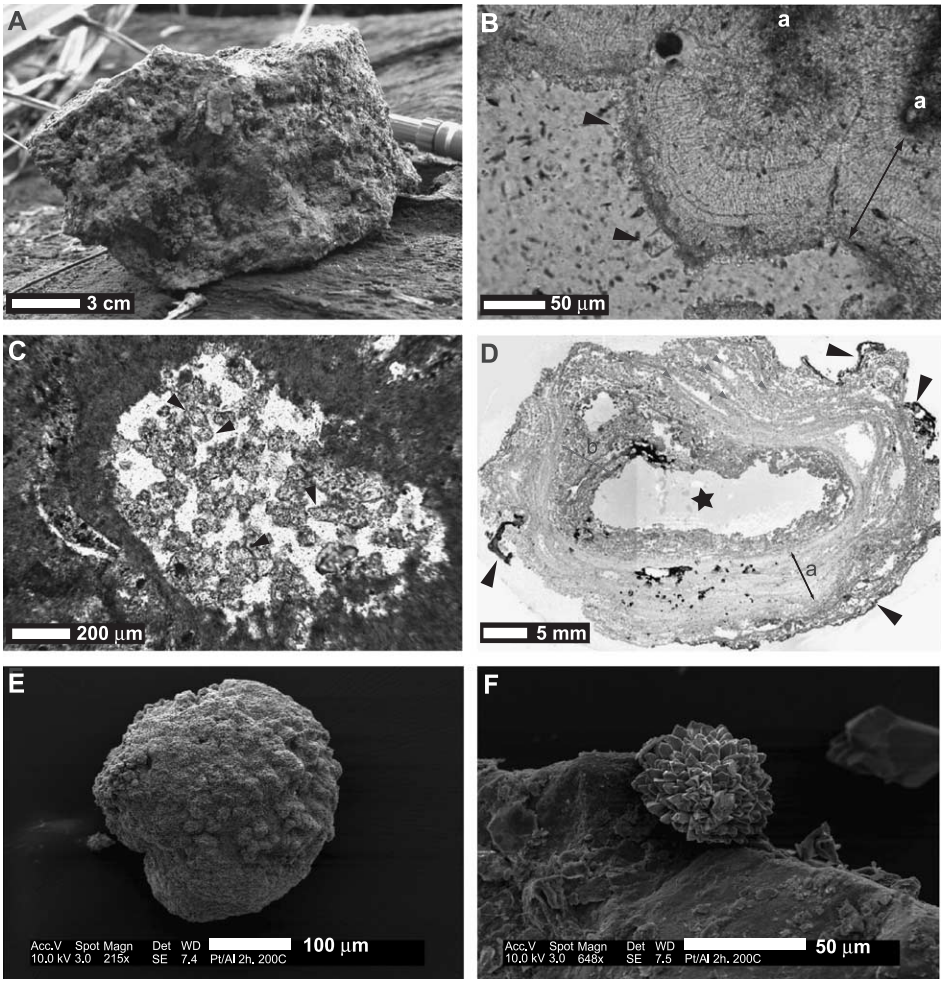

Fig. 7. Large carbonate block features (A – F). (A) Large block of calcium carbonate found in Profile A. (B) Plane polarized light (PPL) thin section micrograph showing three different calcitic textures: initial micrite (a); finely laminated radiaxial fibrous cement (double headed arrow); micro-sparitic to sparitic semi-translucent cement with a locally palisadic arrangement (black arrows). (C) Cluster of rhombohedra at 30-cm depth (black arrows). They are identified as Type I because of their translucent texture and size (approximately 100 μm). (D) Transverse cross-section of a large block. Wood tissues are observed in the periphery of the block (black arrows). Concentric laminations (small arrows) are found in the partially calcified outer part of the sample (double headed arrow and a) and are generally in contact with wood tissues; these tissues constitute the boundary between the blocks and the orthox soil matrix. The inner part of the block has a clotted fabric with a micritic texture (double headed arrow and b). Star: central void. (E, F) SEM micrographs: (E) micritic aggregate found in the top of Profile A as well as in the sap. (F) Vaterite hemi-spherulite growing on a silica substrate.

successive layers are concentric (Fig. 7D), disappearing from the external surface of the sample to its inner part, which exhibits a granular texture. The centre of the sample is hollow.

4.5. Micritic aggregates and hemi-spherulites

Micritic aggregates are found in the sap on the trunk as well as in the profile below the tree to a depth of 40 cm. These features consist of micrite grains agglomerated in irregular masses (Fig. 7E). They can also form porous micritic spherical aggregates, embedded in an exopolysaccharidic biofilm, which gives a soft cohesion to the whole mass.

In some wood fragments (60 cm deep), calcium carbonate hemi-spherulites were found developed on silica grains or on the wood (Fig. 7F). Their mineralogy has not been determined by X-ray diffraction analysis because of the technical impossibility of micro-sampling. These spherulites, 50 μm in size, are virtually identical to those produced by Braissant et al. (2003) in amino acid-enriched media. These spherulites have been identified as vaterite ($CaCO_3$) by the authors.

4.6. Mineralogy

X-ray diffraction has been used to determine the mineralogy of carbonate accumulations in Profile A, some selected samples of Profile B, and some fragments of buried mineralized wood samples (to a depth of 60 cm). Mineralized wood tissues such as calcitic cellulose fiber pseudomorphoses, bulk calcified wood tissues, and vessel infillings have a strictly stoichiometric calcitic signature. In one sample, monohydrocalcite has been detected (at 50 cm in depth; Fig. 8A). In Profile A, some samples exhibit a dissymmetric peak attesting to the presence of more than one type of calcite. The shoulder area, visible at the base of the peak, indicates the presence of a stoichiometric calcite and two other carbonate polymorphs variously enriched in magnesium. In addition, oxalate crystals identified as weddellite have been found in soil samples in the upper 20 cm of Profile A. X-ray diffraction analysis also indicates the presence of whewellite in wood fragments at a depth of 60 cm (Fig. 8B).

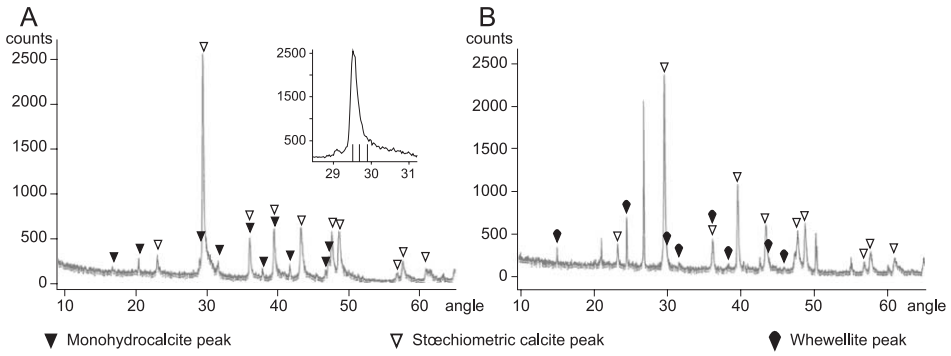

Fig. 8. (A) X-ray diffractogram of a mineralized wood sample (5-cm depth, Profile A) showing the presence of monohydrocalcite. The dissymmetric peak of calcite (104) has been treated by deconvolution, emphasizing the presence of three calcite polymorphs: a stoichiometric calcite (uncorrected peak at 29.50) and two Mg-calcites (uncorrected peaks at 29.68 and 29.89). (B) Whewellite in a partially mineralized wood fragment found at 60-cm depth in Profile A.

4.7. Calcium carbonate distribution in the soil

The O and A horizons are characterized by a 12% to 14% calcium carbonate content. In these horizons, two morphologies of $CaCO_3$ were observed: wood tissues and Types I and II rhombohedra. Wood tissues are the most important features to contribute to calcium carbonate accumulation, although the rhombohedra's contribution is not negligible. The B_k horizon is characterized by various calcium carbonate forms: large blocks are often composed of 90% to 96% of $CaCO_3$, whereas soft soil samples have a $CaCO_3$ content between 2.5% and 16.5%. All the morphologies that are described in this study (Types II and III rhombohedra, needle fiber calcite and blocks) are mostly concentrated in this horizon. Wood tissues disappear progressively with depth. Below the B_k horizon, B and BC horizons are characterized by low amounts of $CaCO_3$ (between 0% and 2%). Below the decrease in carbonate content noted at the base of the B_k horizon, $CaCO_3$ totally disappears in the lower part of the B horizon. Nevertheless, between a depth of 75 and 85 cm, the calcium carbonate content is slightly >0%, mainly due to the presence of Type III rhombohedra and locally, NFC. This distribution is summarized in Fig. 9.

4.8. Calcium input

Three sources of calcium have been identified: (i) the parent rock, a calco-alkaline granite, can provide between 0.03 and 1.43 kg/ha/year of calcium depending on weathering rate and calcium content; (ii) analysis of two Biga rain samples allowed us

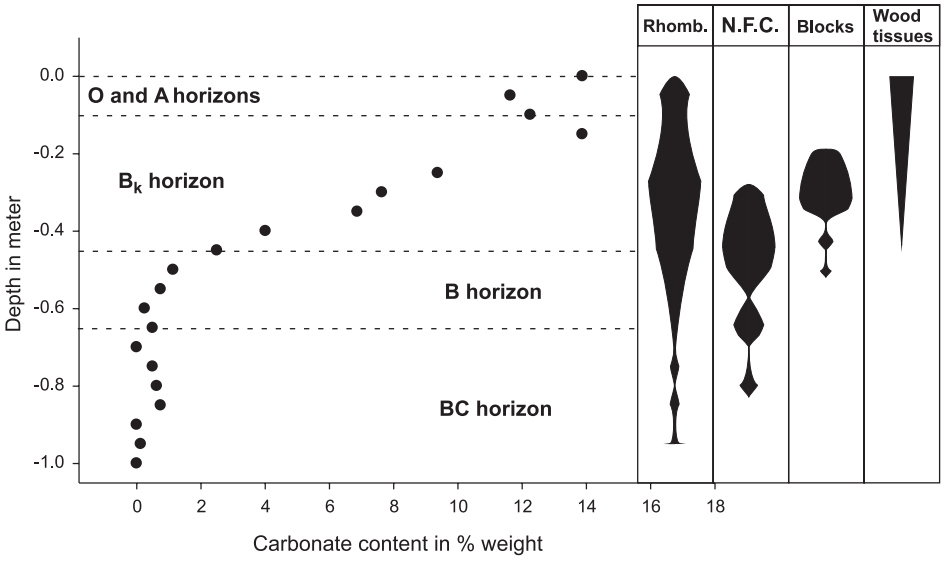

Fig. 9. Distribution of calcium carbonate content along Profile A and relative distribution of the most important $CaCO_3$ features. Comparison between feature concentrations is relative (thickness is not related to scale). Rhomb: rhombohedra; NFC: needle fiber calcite; Blocks: large $CaCO_3$ blocks; Wood tissues: $CaCO_3$ wood pseudomorphoses.

Depth in m	pH
-0.05	8.87
-0.15	8.16
-0.25	8.60
-0.35	8.99
-0.40	8.57
-0.50	8.54
-0.55	8.66
-0.65	8.84
-0.70	8.72
-0.75	8.61
-0.85	8.57
-0.95	8.44

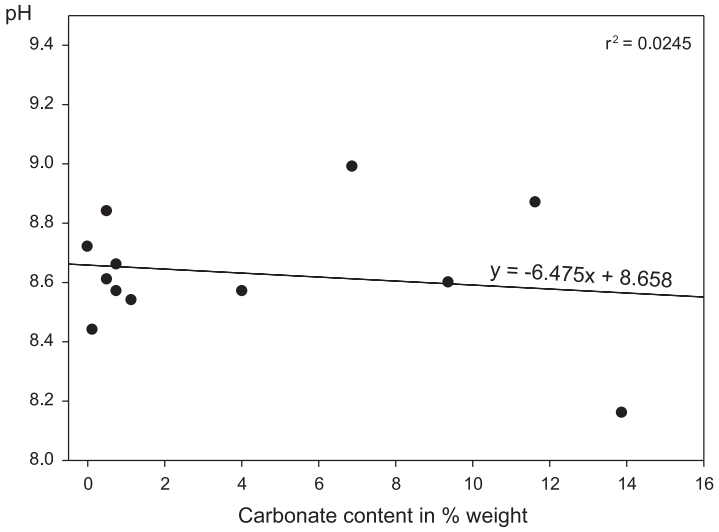

Fig. 10. Distribution of pH vs. depth. Scatterplot of carbonate content in % weight vs. pH. The regression line calculated using these data is characterized by a very low $r^2 = 0.0245$. There is no relationship between pH and carbonate content.

to determine that 5.4–4.8 kg/ha/year of calcium is provided to the soil. This value is in agreement with a previous average of 6.5 kg/ha/year of calcium determined from 19 rains (Stoorvogel et al., 1997); (iii) during the dry season, a large amount of dust from the Harmattan wind provides 3.5 kg/ha/year of calcium (Stoorvogel et al., 1997). In addition, soil extracts from two layers of Profile A (5- and 30-cm depth) contain 28 and 62 ppm of calcium, respectively.

4.9. Relationship between pH and calcium carbonate content

Soil pH ranges from 8.16 to 8.99 (Fig. 10). Except for one sample (15 cm deep), all measurements display a pH>8.4 (stability pH of calcite at $pCO_2 = 3.43 \times 10^{-4}$ atm and $T = 25$ °C). The pH commonly measured in orthox soils from Ivory Coast developed on calco-alkaline granite parent rock is between 4.3 and 6 (Leneuf, 1959). In addition, rainwater sampled in the Daloa region had a pH ≈ 4.7. The scatterplot of carbonate content in % weight vs. pH (Fig. 10) shows no relationship between pH and $CaCO_3$ content ($r^2 = 0.0245$).

5. Discussion

The pH of orthox soils in Ivory Coast has been measured to be between 4.3 and 6 (Leneuf, 1959). Surprisingly, calcium carbonate has been found in Biga soils where the pH is not supposed to be favorable for calcite precipitation. In addition, oxalate crystals have been detected in soil samples, wood tissues, and associated with Actinomycetes

(Fig. 11A–D). Is there a relationship between the presence of oxalate and $CaCO_3$ precipitation?

Some recent experimental work has emphasized the important role of soil bacteria in the consumption of oxalate, resulting in carbonate precipitation and increase in pH (Braissant et al., 2002). It has been shown that oxidation of oxalate by bacteria (such as

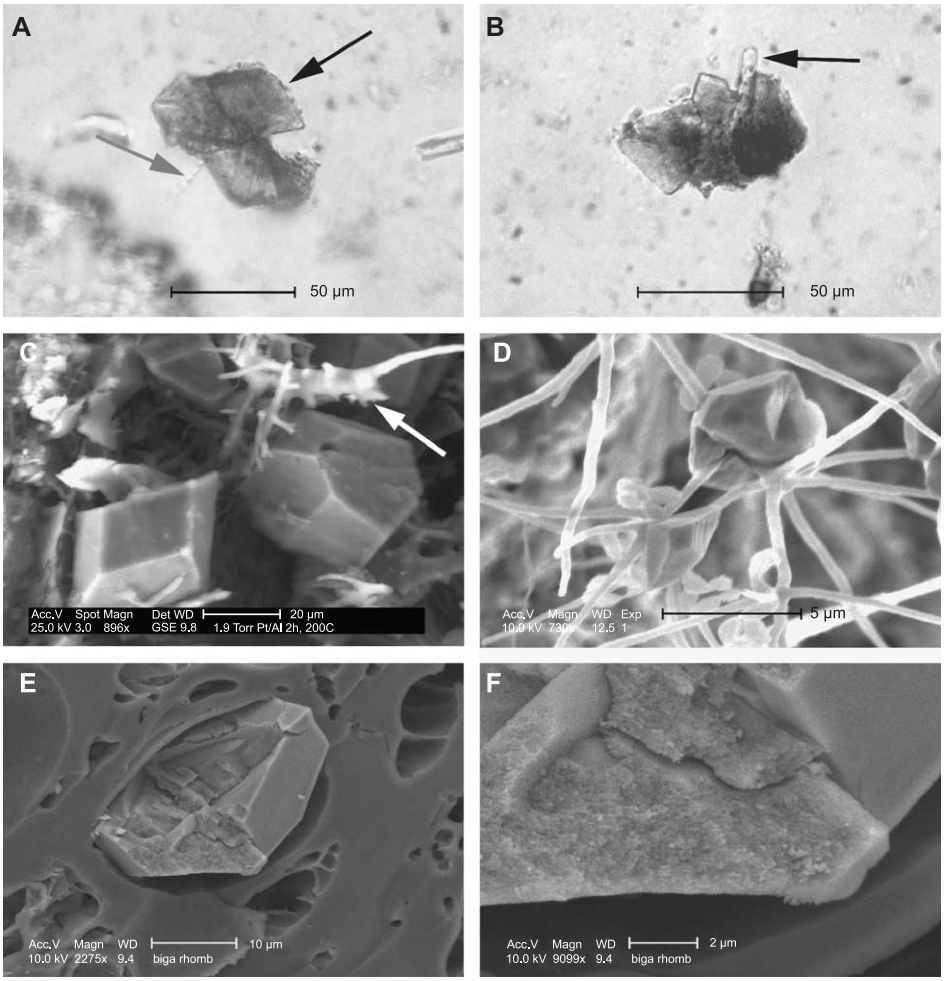

Fig. 11. (A, B) PPL micrographs under binocular: weddellite crystals found associated with rhombohedra in the upper 15 cm of Profile A. Black arrows show different weddellite habits; (A) bipyramidal habit, (B) rod habit. Grey arrow: microorganic filament. (C–F) SEM micrographs. (C) Oxalate crystals found in a wood fragment of the Profile A at 60 cm in depth (arrow: fungal filaments). (D) Oxalate crystal associated with nocardioform soil bacteria at 5 cm in depth (Profile A). (E, F) Cryo-SEM micrographs of calcite crystal obtained experimentally by burning iroko bark at 500 °C. (E) Calcite crystal broken along fractures during cryo-preparation; the fractures appear during oxalate–carbonate transformation. (F) Detail of the internal structure of calcitic pseudomorphic crystal of oxalate composed of stacked nanospheres.

Ralstonia eutropha and *Xanthobacter autotrophicus*) induced an increase in pH in the medium of up to 9.5, which is the value determined by theoretical calculations. This process probably strongly contributes to increase the pH in Biga soils, as well as calcite precipitation, iroko trees being an important source of oxalate (Braissant et al., 2004).

Regarding the calcium carbonate features, X-ray diffraction allowed the identification of various degrees of magnesium-enriched calcite in the $CaCO_3$ solid solution. The formula of three polymorphs have been calculated from peak deconvolution following Kübler's (1992) method: (i) $CaCO_3$, (ii) $Ca_{0.94-0.93}$, $Mg_{0.06-0.07}CO_3$, and (iii) $Ca_{0.87-0.85}$, $Mg_{0.13-0.15}CO_3$ (Fig. 8A). In some samples, monohydrocalcite has also been detected associated with the calcite polymorphs (Fig. 8A). Individual magnesian-enriched calcite crystals have not been sampled because it is impossible to see a morphological difference between the various polymorphs. The origin of Mg-enriched calcite polymorphs is still unclear. Nevertheless, they can be linked to the presence of monohydrocalcite, which includes Mg-rich fluid inclusions. In addition, monohydrocalcite is assumed to be a precursor to magnesian-enriched calcite (Taylor, 1975; Skinner et al., 1977).

The atypical texture of Type II rhombohedra is similar to some of the crystals observed by Canti (2003) in plant ashes. This atypical texture is produced by the transformation of oxalate crystals into carbonate during burning. A temperature of 470 °C must be reached for the oxalate–carbonate transformation in a forest fire. Burning an iroko bark fragment produced crystals similar to soil rhombohedra (Fig. 11E–F). Type II rhombohedra must be interpreted as the result of natural or anthropic fires, which are common in Africa. Type III rhombohedra are the result of epitactic growth of calcite on Type II rhombohedra. The distribution of Types II and III rhombohedra in the soil is probably due to bioturbation by termites and/or ants.

Regarding needle-fiber calcite, its origin (inorganic or biological) has been discussed for a long time. Inorganic origin is possible when precipitation occurs from highly supersaturated solutions obtained during rapid evaporation, which leads to crystals with atypical shapes such as dendrites, needles, and whisker crystals (James, 1972; Riche et al., 1982; Jones and Ng, 1988; Jones and Kahle, 1993; Borsato et al., 2000). Nevertheless, highly supersaturated solutions can also be locally obtained during root activity and exchanges in the rhizosphere between root cells and soil solutions. This kind of supersaturation allows precipitation of calcite crystals with long habits (Harrison, 1977). A direct biologic origin for needle fiber calcite has also been proposed by Callot et al. (1985a,b), Verrecchia and Verrecchia (1994), Newman et al. (1996), Loisy et al. (1999), and Monger and Gallegos (2000). Needles are assumed to precipitate in fungal cell walls and to be released during biological decay or during soil moisture deficiency, leading to the hyphae bursting. M microrods similar to those described by Verrecchia and Verrecchia (1994) have been found in Profile A. They are probably microbial in origin, produced by threadlike and baciliform bacteria (Loisy et al., 1999).

Furthermore, the role of bacteria can also be emphasized for micritic aggregate genesis. Experimental work, in which oxalate consumption by *X. autotrophicus* was tested in a Biga soil-extract medium (Fig. 12A), produced micritic aggregates identical in shape and mineralogy to those found at the Biga site (compare Figs. 7E and 12A). Vaterite hemi-spherulites were also synthesized in amino acid-enriched media (Braissant et al., 2003). These synthetic hemi-spherulites (Fig. 12B) can be compared with natural hemi-spher-

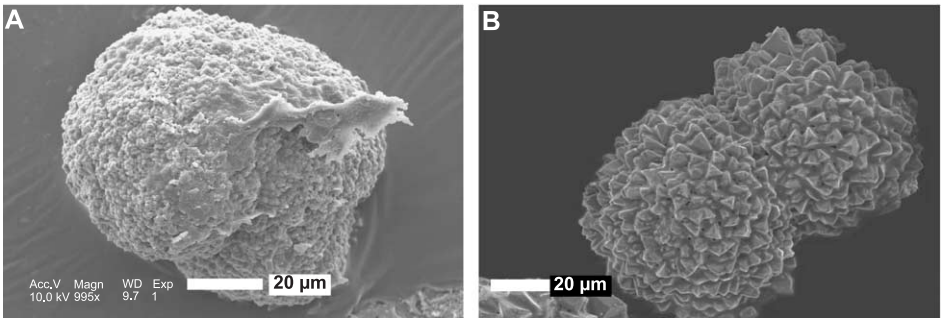

Fig. 12. SEM micrographs of spherulites. (A, B) Experimental $CaCO_3$ products. (A) Micritic aggregate produced on a Biga site soil-extract medium inoculated with *X. autotrophicus*. (B) Vaterite hemi-spherulites produced in the presence of L-aspartate (Braissant et al., 2003).

ulites found in sap (Fig. 7F), emphasizing the potential role of organic molecules in their genesis.

Two hypotheses can be proposed to explain why no quartz grains were found in the large blocks of calcium carbonate. (i) The silica and ferruginous phases have been dissolved when calcium carbonate accumulation occurred. This could explain the absence of a silica phase but in the samples found at >50-cm depth, quartz grains are pluri-millimetric in size, and thus, it seems difficult to dissolve them. This hypothesis is unlikely and must be rejected. (ii) The calcium carbonate precipitates in a soil cavity, formed during wood fragment decay. The cavity can be enlarged posteriorly to the precipitation of the first calcite generation.

This hypothesis explains the preservation of the macro-void and the concentric and centripetal features. Organic material constitutes a framework for a first generation of cement, and after the disappearance of this framework, other generations can precipitate above and below the pre-existing calcitic fans. The numerous laminations, visible in the calcite cement, reveal a polyphased genesis. Therefore, large blocks found at the Biga site are likely to be the result of pre-mineralization of the outer wood structure, as has been described for the trunk itself (Braissant et al., 2004). When the inner wood tissues are decayed by soil organisms (in particular, termites), the mineralized outer structure can preserve a hollow space. A secondary centripetal calcium carbonate accumulation can plug this macro-porosity.

6. Conclusions

Calcium carbonate accumulations at the Biga site are found in many forms, ranging from euhedral crystals to large blocks with various textures. Different genetic factors have been inferred for these various forms. The presence of hemi-spherulites found in sap, and similar ones produced by experimental work (Braissant et al., 2003), stresses the role of exopolysaccharides and amino acids in calcium carbonate precipitation. Moreover, the link between micritic aggregates, oxalate, and soil bacteria seems established by experimental

work (Braissant et al., 2002). For example, the consumption of oxalate by soil bacteria on a Biga soil-extract medium has been observed and has led to micritic aggregate precipitations similar to those found at the natural Biga site. Moreover, some rhombohedra have been interpreted as the result of forest fire, natural or not, inducing oxalate–carbonate pseudomorphoses.

Even if very large blocks described by Carozzi (1967) have not been found at the Biga site, another type of block has been observed in this study. These large blocks of quartz-free carbonate are not the result of lithification of a pre-existing soil matrix like those found by Carozzi (1967). They are the remains of buried wood and root fragments, which underwent secondary calcium carbonate mineralization.

Calcium carbonate accumulation can occur in orthox acidic equatorial soils, showing that these soils can be locally alkaline. The presence of oxalate in the soil creates favorable conditions for $CaCO_3$ precipitation. During oxalate oxidation into carbonate by soil flora, the pH increases, allowing the reaction of carbonate species (HCO_3^-, CO_3^{2-}) with free Ca^{2+}, followed by the enhancement of calcium carbonate precipitation. It seems that a period of low rainfall is necessary to allow $CaCO_3$ accumulation in the upper soil. Moreover, the amount of $CaCO_3$ increases due to carbonate mineralization of the iroko tree itself. To summarize, three conditions seem necessary for calcium carbonate accumulations in orthox soils: (i) a large amount of oxalate, (ii) an oxalotrophic flora for oxalate oxidation into carbonate and (iii) a dry season.

Acknowledgements

The authors wish to thank the two reviewers, Professors G. Stoops and A. Yaïr, who greatly improved the first draft of this manuscript. CSRS (Swiss Science Research Centre, Abidjan, Ivory Coast) and Mr. E. Bomisso (Université de Cocody, Abidjan, Ivory Coast) provided help in the field. This work is supported by the Swiss National Science Foundation, grant no 2153-065174.01.

References

Borsato, A., Frisia, S., Jones, B., Van Der Borg, K., 2000. Calcite moonmilk: crystal morphology and environment of formation in caves in the Italian Alps. Journal of Sedimentary Research 70, 1179–1190.

Braissant, O., Verrecchia, E.P., Aragno, M., 2002. Is the contribution of bacteria to terrestrial carbon budget greatly underestimated? Naturwissenschaften 89, 366–370.

Braissant, O., Cailleau, G., Dupraz, C., Verrecchia, E.P., 2003. Bacterially induced mineralization of calcium carbonate in terrestrial environments: the role of exopolysaccharides and amino acids. Journal of Sedimentary Research 73, 485–490.

Braissant, O., Cailleau, G., Aragno, M., Verrecchia, E.P., 2004. Biologically induced mineralization in the iroko *Milicia excelsa* (Moraceae): its causes and consequences to the environment. Geobiology 2, 59–66.

Callot, G., Guyon, A., Mousain, D., 1985a. Inter-relation entre les aiguilles de calcite et hyphes mycéliens. Agronomie 5, 209–216.

Callot, G., Mousain, D., Plassard, C., 1985b. Concentrations de carbonate de calcium sur les parois des hyphes mycéliens. Agronomie 5, 143–150.

Campbell, W.G., Fisher, R.C., 1932. The composition and origin of "stone" in Iroko wood (*Chlorophora excelsa* Benth. and Hook. f.). Empire Forestry Journal 11, 244–245.

Canti, M.G., 2003. Aspects of the chemical and microscopic characteristics of plant ashes found in archaeological soils. Catena 54, 339–361.

Carozzi, A.V., 1967. Recent calcite-cemented sandstone generated by the equatorial tree iroko (*Chlorophora excelsa*), Daloa, Ivory Coast. Journal of Sedimentary Petrology 37 (2), 597–600.

FAO, 2001. http://www.fao.org/giews/french/basedocs/ivc/ivcmet1f.stm.

Harris, C.M., 1933. Stone in *Chlorophora excelsa* B. and H. Iroko. Empire Forestry Journal 12, 229–238.

Harrison, R.S., 1977. Caliches profiles: indicator of near-surface subaerial diagenesis, Barbados West Indies. Bulletin of Canadian Petroleum Geology 25, 123–173.

James, N.P., 1972. Holocene and Pleistocene calcareous crust (caliche) profiles: criteria for subaerial exposure. Journal of Sedimentary Petrology 42, 817–836.

Jones, B., Kahle, C.F., 1993. Morphology, relationship, and origin of fiber and dendrite calcite crystals. Journal of Sedimentary Petrology 63, 1018–1031.

Jones, B., Ng, K.C., 1988. The structure and diagenesis of rhizoliths from Cayman Brac, British West Indies. Journal of Sedimentary Petrology 58, 457–467.

Kübler, B., 1992. Calcites magnésiennes: identification et dosage par diffraction X de $MgCO_3$ dans la solution solide. Cahiers de l'Institut de Géologie, Laboratoire de Minéralogie, Pétrographie et Géochimie; Université de Neuchâtel, Institut de Géologie série AX, N.22, 15 pp.

Leneuf, N., 1959. L'altération des granites calco-alcalins en Côte d'Ivoire forestière et les sols qui en sont dérivés O.R.S.T.O.M, Paris 210 p.

Loisy, C., Verrecchia, E.P., Dufour, P., 1999. Microbial origin for pedogenic micrite associated with a carbonate paleosol (Champagne, France). Sedimentary Geology 126, 193–204.

Monger, H.C., Gallegos, R.A., 2000. Biotic and abiotic processes and rates of pedogenic carbonate accumulation in the Southwestern United States—relationship to atmospheric CO_2 sequestration. In: Lal, R., Kimble, J.M., Eswaran, H., Stewart, B.A. (Eds.), Global climate change and pedogenic carbonates. Lewis Publishers, Boca Raton, pp. 273–289.

Newman, B.D., Norman, D.I., Gundimeda, M., Levy, S.S., 1996. Understanding the genesis of nonmarine calcite deposits through quadrupole mass spectrometric analysis of fluid inclusion gases. Chemical Geology 132, 205–213.

Riche, G., Rambaud, D., Riera, M., 1982. Etude morphologique d'un encroûtement calcaire, Région d'Irecê, Bahia, Brésil. Cahiers Orstom. Série Pédologie 19, 257–270.

Skinner, H.C.W., Osbaldiston, G.W., Wilner, A.N., 1977. Monohydrocalcite in a guinea-pig bladder stone, a novel occurrence. American Mineralogist 62, 273–277.

Stoorvogel, J.J., Van Breemen, N., Janssen, B.H., 1997. The nutrient budgets of a watershed and its forest ecosystem in the Taï National Park in Côte d'Ivoire. Biogeochemistry 37, 159–172.

Taylor, G.F., 1975. The occurrence of monohydrocalcite in two small lakes in the southeast of South Australia. American Mineralogist 60, 690–697.

Teeuw, R.M., 2002. Regolith and diamond deposits around Tortiya, Ivory Coast, West Africa. Catena 49, 111–127.

Verrecchia, E.P., Verrecchia, K., 1994. Needle-fiber calcite: a critical review and a proposed classification. Journal of Sedimentary Reseach A64, 650–664.